Negative refractive index metamaterials from inherently non-magnetic materials for deep infrared to terahertz frequency ranges

2005 J. Phys.: Condens. Matter 17 3717

(http://iopscience.iop.org/0953-8984/17/25/002)

INSTITUTE OF PHYSICS PUBLISHING JOURNAL OF PHYSICS: CONDENSED MATTER

J. Phys.: Condens. Matter **17** (2005) 3717–3734 doi:10.1088/0953-8984/17/25/002

Negative refractive index metamaterials from inherently non-magnetic materials for deep infrared to terahertz frequency ranges

Vassilios Yannopapas[1] **and Alexander Moroz**[2]

[1] Department of Materials Science, School of Natural Sciences, University of Patras, GR-26504 Patras, Greece
[2] Wave-scattering.com

E-mail: vyannop@upatras.gr and wavescattering@yahoo.com (A Moroz)

Received 9 February 2005
Published 10 June 2005
Online at stacks.iop.org/JPhysCM/17/3717

Abstract
We present a new set of artificial structures which can exhibit a negative refractive index band in excess of 6% in a broad frequency range from the deep infrared to the terahertz region. The structures are composites of two different kinds of non-overlapping spheres, one made from inherently non-magnetic polaritonic and the other from a Drude-like material. The polaritonic spheres are responsible for the existence of negative effective magnetic permeability whilst the Drude-like spheres are responsible for negative effective electric permittivity. The resulting negative refractive index structures are truly subwavelength structures with wavelength-to-structure ratio 14:1, which is almost 50% higher than has been previously achieved. Our results are explained in the context of the extended Maxwell–Garnett theory and are reproduced by calculations based on the layer Korringa–Kohn–Rostoker method, an *ab initio* multiple scattering theory. The role of absorption in the constituent materials is discussed. Effective medium computer F77 code is freely available at http://www.wave-scattering.com

1. Introduction

Metamaterials constitute a new class of artificial composite materials which possess magnetic properties in frequency regions otherwise not accessible to homogeneous materials, or they exhibit negative electric permittivity and magnetic permeability simultaneously, resulting in a negative refractive index. Mere magnetic response of materials at terahertz and infrared frequencies is important for the implementation of devices such as compact cavities, adaptive selective lenses, tunable mirrors, isolators, converters, optical polarizers, filters, and phase shifters [1, 2]. Negative refractive index metamaterials introduce a new realm of phenomena in optics which stem from negative refraction: superlensing, near-field imaging and amplification, cavity super-resonance, highly selective frequency filters, optical multiplexers, as well as frequency-tunable beam narrowing, focusing and expanding devices [3–5]. Negative refractive index metamaterials were predicted theoretically by Veselago [3] and Silin [4] a few decades ago [6], and both *theoretically* explained (in terms of wave-vector diagrams) and *experimentally* verified (in the case of a doubly periodic planar waveguide between unmodulated regions with parallel straight boundaries in the visible) by Zengerle [7]. However, it was not until a publication by Pendry [8] that the subject of negative refractive index materials became a rapidly growing field.

Negative refractive index metamaterials come in two basic designs, namely those based on purely dielectric periodic structures [7, 9, 10], or as periodic metallic microstructures exhibiting electric [11, 12] and magnetic [13] resonances [4, 14–18]. The purely dielectric metamaterials [7, 9, 10] are characterized by rather low wavelength-to-structure ratio (typically less than 2:1). On the other hand, metamaterials based on metallic microstructures, the most prominent example of which are those consisting of split ring resonators (SRRs) and wires [14–19], are truly subwavelength structures with wavelength-to-structure ratio at least 5:1. In this paper we propose a metallo-dielectric structure of much simpler geometry than the common metamaterials (SRRs and wires) which exhibits a frequency band of negative refractive index. The favoured realization of our structure is a *periodic* crystal wherein polaritonic spheres and Drude-like or plasma spheres are arranged on two interpenetrating *simple cubic* lattices, respectively. When the differences between the spheres are ignored, the resulting structure is a face-centred cubic (fcc) structure. We consider in detail the so-called [001] direction of the fcc lattice. This means that the respective spheres will form alternating two-dimensional photonic crystal layers which, from a geometric point of view, are identical *square* lattices. The sublattice of polaritonic spheres possesses negative magnetic permeability in certain frequency regions while the sublattice of the Drude-like spheres possesses negative electric permittivity. Both phenomena are the result of the strong single sphere Mie resonances. By suitable choice of materials and parameters, a common region can be found, within a broad frequency range from the deep infrared to the terahertz region, where both functions are negative and the structure exhibits a negative refractive index band in excess of 6% bandwidth. The resulting negative refractive index structure is a truly subwavelength structure with wavelength-to-structure ratio as high as 14:1, which is almost 50% higher than has been previously achieved [14–18]. Therefore, our structure is expected to be more robust against disorder. In fact, we shall present some indications that the negative refractive index band may even survive in the presence of disorder.

The outline of the paper is as follows. Section 2 illustrates how an effective magnetic permeability of composites of inherently *non-magnetic* spherical particles arises within the context of an extended Maxwell–Garnett theory [20, 21]. In section 3 the magnetic properties of three-dimensional photonic crystal of polaritonic spheres are investigated. Section 4 then describes the proposed periodic realizations of the negative refractive index structures. The effective medium properties are studied both using the extended Maxwell–Garnett theory and a photonic version of the layer Korringa–Kohn–Rostoker (LKKR) method, which is based on rigorous multiple-scattering theory, using a well documented computer code [22–24]. The influence of absorption of the constituent materials on the properties of the resulting structure is studied in section 5. The origin of negative refractive index band, related work, fabrication, aperiodic realizations, and an outlook of possible alternative realizations of negative refractive index structures with high wavelength-to-structure ratios are all discussed in section 6. Section 7 then concludes the paper.

2. Effective medium approach

The essential part in the study of the proposed metamaterial is the effective medium approach which will provide us with the effective permittivities and permeabilities. Let us consider a composite of spheres with relative dielectric permittivity ϵ_s and magnetic permeability μ_s, embedded in a host medium described by a relative dielectric permittivity ϵ_h and magnetic permeability μ_h. With f we denote the volume filling fraction occupied by the spheres in the composite and x will stand for the sphere size parameter, $x \equiv \sqrt{\epsilon_h \mu_h}\omega S/c = 2\pi S/\lambda$, where S denotes the sphere radius and λ is the wavelength in the host medium. Let us also define $x_s \equiv \sqrt{\epsilon_s \mu_s}\omega S/c = 2\pi S/\lambda_s$, where λ_s is the wavelength in the sphere medium. According to Maxwell–Garnett theory, provided that both $x \ll 1$ and $x_s \ll 1$ (static limit), the effective relative dielectric permittivity ϵ_{eff} of a collection of particles is given by the formula

$$\epsilon_{\text{eff}} = \epsilon_h \frac{1 + 2f\alpha_s}{1 - f\alpha_s}, \tag{1}$$

where $\alpha_s = (\epsilon_s - \epsilon_h)/(\epsilon_s + 2\epsilon_h)$ is the single-sphere polarization factor. Provided that $x \ll 1$ but *not* necessarily $x_s \ll 1$ (the so-called *quasi-static limit*), the static polarization factor α_s in the Maxwell–Garnett formula (1) no longer properly reflects the polarization properties of single particles. The required quasi-static extension of the Maxwell–Garnett formula (1), also known as extended Maxwell–Garnett formula, can be obtained by Mie theory [20, 21],

$$\epsilon_{\text{eff}} = \epsilon_h \frac{x^3 - 3\mathrm{i} f T_1^{\mathrm{E}}}{x^3 + \frac{3}{2}\mathrm{i} f T_1^{\mathrm{E}}}, \tag{2}$$

where T_1^{E} is the electric-dipole component of the scattering T-matrix of a single sphere. Therefore, the quasi-static result (2) differs from the corresponding Maxwell–Garnett static result (1) in the replacement of the static polarization factor $\alpha_s = (\epsilon_s - \epsilon_h)/(\epsilon_s + 2\epsilon_h)$ by the quasi-static (also called renormalized) polarization factor $\alpha_{qs} = -3\mathrm{i}T_1^{\mathrm{E}}/(2x^3)$. The extended Maxwell–Garnett effective relative dielectric permittivity ϵ_{eff} is the leading order in the expansion of the exact effective permittivity of the composite in the powers of the filling fraction f (see equations (33), (35) of [25]). A similar equation for the effective relative magnetic permeability reads

$$\mu_{\text{eff}} = \mu_h \frac{x^3 - 3\mathrm{i} f T_1^{H}}{x^3 + \frac{3}{2}\mathrm{i} f T_1^{H}}, \tag{3}$$

where T_1^H is the magnetic-dipole components of the scattering T-matrix of a single sphere. Explicit expressions of T_1^{E} and T_1^H are given by the following formulae:

$$\begin{aligned} T_1^{\mathrm{E}}(\omega) &= \left[\frac{j_1(x_s)\,[xj_1(x)]'\,\epsilon_s - j_1(x)\,[x_s j_1(x_s)]'\,\epsilon_h}{h_1^+(x)\,[x_s j_1(x_s)]'\,\epsilon_h - j_1(x_s)\left[xh_1^+(x)\right]'\epsilon_s}\right], \\ T_1^{H}(\omega) &= \left[\frac{j_1(x_s)\,[xj_1(x)]'\,\mu_s - j_1(x)\,[x_s j_1(x_s)]'\,\mu_h}{h_1^+(x)\,[x_s j_1(x_s)]'\,\mu_h - j_1(x_s)\left[xh_1^+(x)\right]'\mu_s}\right], \end{aligned} \tag{4}$$

where $j_1(h_1^+)$ is the spherical Bessel (Hankel) function for $l = 1$ and $[xj_1(x)]' = \mathrm{d}[zj_1(z)]/\mathrm{d}z|_{z=x}$, etc.

Note in passing the following observations. First, equation (2) reduces to the Maxwell–Garnett result (1) in the limit $x_s \ll 1$. Second, if the spherical Bessel and Hankel functions in T_1^{E} and T_1^H are expressed in terms of sines and cosines (see, for example, equations (10.1.11–12) of [26]), the above expressions (2) and (3) for the effective relative dielectric permittivity and magnetic permeability can be shown to be identical to those derived earlier by Lewin [27] (see

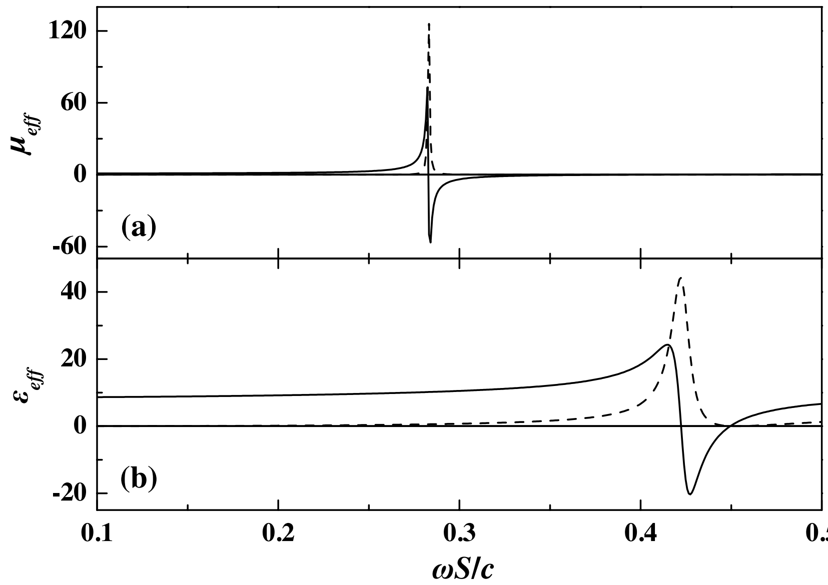

Figure 1. Relative effective permeability μ_{eff} (a) and permittivity ϵ_{eff} (b) as functions of frequency for a three-dimensional fcc crystal of close-packed spheres with $\epsilon_s = 100$, provided by the extended Maxwell–Garnett theory (equations (2)–(4)). The solid (broken) lines correspond to the real (imaginary) parts of μ_{eff} and ϵ_{eff}.

equations (5) and (11) therein) and recently employed by Holloway *et al* [28] (see equations (1)–(6) therein). Third, unlike in the static limit, the effective medium parameters in the quasi-static limit are *dispersive* even for a medium composed of *non-dispersive* components. Fourth, the standard and the extended Maxwell–Garnett effective constants can be used to calculate all the optical properties of the composite medium. In particular, the effective refractive index $n_{\mathrm{eff}} = \sqrt{\epsilon_{\mathrm{eff}}\mu_{\mathrm{eff}}}$ can be substituted in the Snell law to calculate the refraction of incident waves. However, as first noted by Bohren [29] (see also section 4 of [21]), the extended Maxwell–Garnett effective constants obtained in the quasi-static case are complex even in the case of *non-absorbing* spheres embedded in a *non-absorbing* medium. In the latter case, the imaginary part of the effective dielectric constants is associated with the extinction of the propagating beam due to scattering. Therefore, although the extended Maxwell–Garnett effective constants can be used to calculate all the optical properties of the medium, they cannot be used directly to evaluate the absorption or the heating rate [21, 29].

In a composite structure such as the one we consider here, a frequency region where both μ_{eff} and ϵ_{eff} are negative is sufficient for a negative refractive index metamaterial behaviour. As we will demonstrate below, this can be achieved in frequency regions where both T_1^{E} and T_1^{H} exhibit strong resonances such as Mie resonances and surface plasmons. We consider an fcc crystal with period a consisting of dielectric spheres with relative dielectric function $\epsilon_S = 100$ and radius $S/a_0 = 0.5$, where a_0 is the first neighbours' distance. The period, or the lattice constant in the following, is the length of the side of the conventional unit cell of a cubic lattice, so $a_0 = a/\sqrt{2}$ [30]. The particular choice of the crystal structure is not important as long as we are working in the long-wavelength limit and the crystal has cubic symmetry. The latter conditions ensure that the effective medium is *homogeneous* and *isotropic*. The effective relative permittivity and permeability of the above composite are shown in figure 1. It is obvious that there are regions where ϵ_{eff} and μ_{eff} have negative real parts as a result of the Mie resonances occurring in these regions. The magnetic activity in the region of the Mie resonance is a result of the enhancement of the displacement current inside each sphere which, in turn, gives rise to a macroscopic magnetization of the crystal. The electric activity is attributed to the large polarization induced to each sphere due to their enormous dielectric permittivity (see below). Note that, as expected from Mie theory, the magnetic resonance is much sharper than the electric one, implying a longer lifetime of the corresponding virtual bound state (Mie resonance). In order to obtain a frequency region of negative refractive index, our guiding principle, as in earlier work, is to have both ϵ_{eff} and μ_{eff} negative (see, however, section 6.1). Unfortunately, the regions where the corresponding real parts of ϵ_{eff} and μ_{eff} are negative do not overlap. However, the above structure can be a guide to realizing a composite structure which will act as a metamaterial with negative refractive index. Very large values of the relative dielectric permittivity such as the one considered above have been reported in the microwave regime for materials combining ferroelectric $\mathrm{Ba_{0.6}Sr_{0.4}TiO_3}$ (BSTO) with non-electrically active oxide ceramics [31, 32]. But similar values of the relative dielectric permittivity can be also found in more conventional materials such as phonon–polariton materials which will be the case study in the next section. We mention that a similar magnetic activity in photonic crystals has been reported for two-dimensional crystals consisting of dielectric cylinders with $\epsilon = 200$ [31], for particular metal–dielectric composites [1], as well as for three-dimensional crystals of spherical inclusions [28, 33].

3. Three-dimensional polaritonic photonic crystal

As stated above, although photonic structures consisting of high-refractive-index particles are, theoretically, a good candidate for a magnetic metamaterial, i.e., a material whose effective permeability takes on negative values in a certain frequency window, we have chosen a more common type of photonic system. More specifically, we consider the case of a three-dimensional photonic crystal consisting of polariton spheres in air, i.e., spheres whose relative dielectric permittivity is described by

$$\epsilon(\omega) = \epsilon_\infty\left(1 + \frac{\omega_{\mathrm{L}}^2 - \omega_{\mathrm{T}}^2}{\omega_{\mathrm{T}}^2 - \omega^2 - \mathrm{i}\omega\gamma_1}\right), \tag{5}$$

where ϵ_∞ is the asymptotic value of the dielectric permittivity at high frequencies, γ_1 is the loss factor, and the respective ω_{T} and ω_{L} are the transverse and longitudinal optical phonon frequencies. The latter are related by the Sachs–Teller relation: $\omega_{\mathrm{L}} = \omega_{\mathrm{T}}\sqrt{\epsilon(0)/\epsilon_\infty}$. The dielectric function $\epsilon(\omega)$ is that of a single-resonance Drude–Lorentz model and it satisfies the Kramers–Kronig relations [30].

For the sake of clarity, the losses in the polaritonic material described by equation (5) will be neglected for the time being, i.e., we set $\gamma_1 = 0$. (The influence of absorption of the constituent materials is studied later on in section 5.) Photonic crystals consisting of polaritonic materials exhibit a rich variety of interesting phenomena [34] due to the nature of the dielectric permittivity given by equation (5). Among these phenomena, it has been demonstrated recently that a two-dimensional photonic crystal consisting of polaritonic cylinders behaves as a subwavelength metamaterial with negative effective magnetic permeability [35]. As a polaritonic material, we have chosen $\mathrm{LiTaO_3}$, whose permittivity is given by equation (5) having $\omega_{\mathrm{T}}/2\pi = 26.7$ THz, $\omega_{\mathrm{L}}/2\pi = 46.9$ THz, and $\epsilon_\infty = 13.4$ [30]. The radius of the spheres is $S = 0.446$ μm and they occupy the sites of an fcc lattice with lattice constant $a = 1.264$ μm. Note that the radius of non-overlapping spheres arranged in an fcc lattice satisfies $S \leqslant a/(2\sqrt{2}) \approx 0.446\,89$ μm. Therefore, in the present case, we deal with an almost close-packed fcc structure.

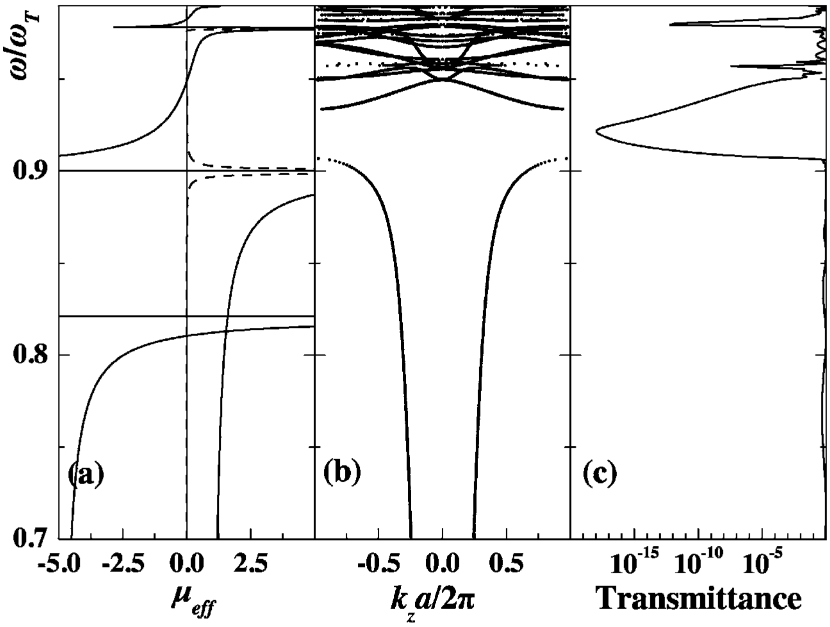

Figure 2. (a) The real (solid line) and imaginary (broken line) parts of $\mu_{\rm eff}$ predicted by the extended Maxwell–Garnett theory and (b) the frequency band structure normal to the (001) surface of an fcc crystal of $LiTaO_3$ spheres ($S = 0.446$ μm, $\omega_{\rm T}/2\pi = 26.7$ THz, $\omega_{\rm L}/2\pi = 46.9$ THz, $\epsilon_\infty = 13.4$) in air as calculated by the rigorous LKKR method. The lattice constant is $a = 1.264$ μm. (c) The corresponding transmittance curve for light incident normally on a slab, 16 layers thick, of the above crystal.

In figure 2(a) we show the relative effective magnetic permeability as calculated by the extended Maxwell–Garnett formulae (3) and (4). We see that there are two regions where the real part of $\mu_{\rm eff}$ is negative: the first region is from $\omega/\omega_{\rm T} = 0.900$ to 0.948 and the second region extends from $\omega/\omega_{\rm T} = 0.978$ to 0.982. As explained in the previous section, these regions correspond to Mie resonances of the isolated $LiTaO_3$ spheres. We will focus our attention on the low-frequency region as it is considerably wider than the high-frequency one. In order to establish the validity of the effective medium predictions of negative effective permeability and/or permittivity, we employ a photonic version of the LKKR method. The latter is based on an *ab initio* multiple scattering theory, using a well documented computer code [22–24]. The LKKR method is ideally suited for the calculation of the transmission, reflection and absorption coefficients of an electromagnetic (EM) wave incident on a composite slab consisting of a number of layers which can be either planes of non-overlapping particles with the same two-dimensional periodicity or homogeneous plates. For each plane of particles, the method calculates the full multipole expansion of the total multiply scattered wave field and deduces the corresponding transmission and reflection matrices in the plane-wave basis. The transmission and reflection matrices of the composite slab are evaluated from those of the constituent layers. By imposing periodic boundary conditions one can also obtain the (complex) frequency band structure of an infinite periodic crystal. The method applies equally well to non-absorbing systems and to absorbing ones. Moreover, in terms of speed, convergence and accuracy, the LKKR method is the best method to treat photonic structures of spherical particles. Its chief advantage over the other existing numerical methods lies in its efficient and reliable treatment of systems containing strongly dispersive materials such as Drude-like and polaritonic materials [36]. Comparison of theory and experiment has been known to be very good [37–40].

We view the crystal as a stack of two-dimensional photonic crystal layers (planes of spheres) parallel to the (001) surface (which we assume parallel to the xy plane) of an fcc lattice. Note in passing that each photonic crystal layer is a two-dimensional square lattice with the lattice constant $a_0 = a/\sqrt{2}$. For any given $\mathbf{k}_\parallel = (k_x, k_y)$, we can calculate the real frequency lines: $k_z = k_z(\omega, \mathbf{k}_\parallel)$. In figure 2(b) we show the frequency band structure, for $\mathbf{k}_\parallel = \mathbf{0}$ (normal to the (001) surface), for the above-mentioned polaritonic photonic crystal. From figure 2(b) we see that the LKKR calculation of the frequency band structure predicts a wide photonic band gap from $\omega/\omega_\mathrm{T} = 0.907$ to 0.934. From $\omega/\omega_\mathrm{T} = 0.934$ to 0.949 there exists a singly degenerate band and as such, transmission of normally incident light is negligibly small over the frequency region of this band (optically inactive band) [22, 41, 42]. Further up from this band, the frequency band structure becomes a complicated mixture of singly and doubly degenerate (optically active) bands and it will not concern us here. Within the region of the gap and of the optically inactive bands, we expect to observe a significantly attenuated transmission of light through finite slabs of the above crystal. Therefore we may assume that we have an effective band gap extending in both regions, i.e., from $\omega/\omega_\mathrm{T} = 0.907$ to 0.949. This effective gap almost coincides with the frequency region over which μ_eff is negative (see above). Next to the band structure, in figure 2(c), we show the transmission coefficient of light incident normally on a slab of the crystal consisting of 16 planes of spheres parallel to the (001) surface. As expected, light transmission is much attenuated within the region of the band gap and of the singly degenerate band while it is of the order of unity in regions where doubly degenerate frequency bands exist. For the results of the LKKR method presented in figure 2 as well as for the figures to follow we have used 13 reciprocal-lattice vectors in the plane wave expansion and angular-momentum cutoff $l_\mathrm{max} = 3$ in the spherical wave expansion.

4. Negative refractive index metamaterial composite of plasma and polaritonic spheres

Our aim is to realize a metamaterial possessing a negative refractive index over a certain frequency window. So, the polaritonic crystal studied above must be combined with another crystal possessing a negative-permittivity band gap which overlaps with the corresponding negative-permeability gap of the polaritonic crystal. As is well known, metallic spheres support surface-plasmon modes which are of electric nature and can naturally lead to a negative ϵ_eff. Unfortunately, the frequency regions over which metallic particles support surface-plasmon resonances are in the optical or near-infrared regime, i.e., much higher than the frequency region where the $LiTaO_3$-polaritonic crystal exhibits negative μ_eff. However, the surface plasmon states are also present in certain semiconductor particles whose bulk plasma frequency lies within the infrared regime. Moreover, the bulk plasma frequency of a semiconductor may be varied by changing the amount of doping. This way we can realize a photonic crystal of plasma spheres with tunable optical properties. One- and two-dimensional plasmonic photonic crystals consisting of semiconductor materials have recently been studied [43, 44], and it has been shown that they exhibit large photonic band gaps in the infrared regime.

4.1. Photonic crystals of non-overlapping plasma spheres

The dielectric function of a semiconductor around the region of the bulk plasma frequency is described by a Drude-type formula

$$\epsilon(\omega) = \epsilon_0\left(1 - \frac{\omega_\mathrm{p}^2}{\omega^2 + \mathrm{i}\omega\gamma_2}\right), \tag{6}$$

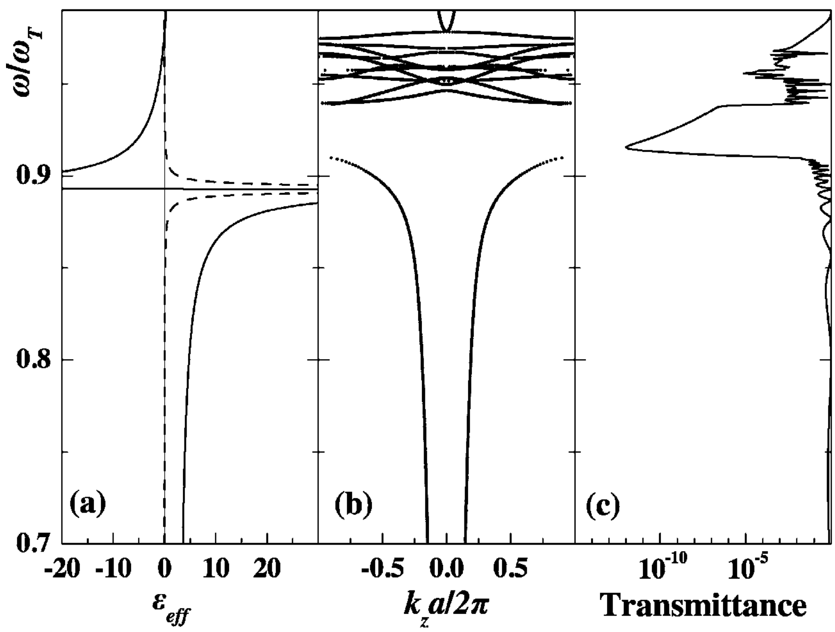

Figure 3. (a) The real (solid line) and imaginary (broken line) parts of $\epsilon_{\rm eff}$ within the extended Maxwell–Garnett theory and (b) the frequency band structure normal to the (001) surface of an fcc crystal of n-type Ge spheres ($S = 0.358\ \mu$m, $\omega_{\rm p}/2\pi = 26.7$ THz, $\epsilon_0 = 15.8$) in air as calculated by the rigorous LKKR method. The lattice constant is $a = 1.264\ \mu$m. (c) The corresponding transmittance curve for light incident normally on a slab, 16 layers thick, of the above crystal.

where $\omega_{\rm p}$ is the bulk plasma frequency of the semiconductor, γ_2 is the loss factor, and ϵ_0 is the static dielectric constant. The Drude dielectric function $\epsilon(\omega)$ can be viewed as a special case of the single-resonance Drude–Lorentz model dielectric function, introduced earlier by equation (5), for $\omega_{\rm T} = 0$. Hence the Drude dielectric function also satisfies the Kramers–Kronig relations. Similarly as in section 3, for the sake of clarity the losses in the equation (6) will be neglected, i.e., we set $\gamma_2 = 0$ for the time being. (The influence of absorption of the constituent materials is studied later on in section 5.) The bulk plasma frequency $\omega_{\rm p}$ is proportional to the square root of the impurity density of the semiconductor [45]. For the formation of a three-dimensional photonic crystal of Drude-like or plasma spheres [36, 46, 47] we choose spheres with the dielectric function of equation (6), where $\omega_{\rm p}$ is the same as $\omega_{\rm T}$ of $LiTaO_3$ and $\epsilon_0 = 15.8$. For n-type Ge, this value of $\omega_{\rm p}$ corresponds to an impurity density $N = 1.34 \times 10^{19}$ cm^{-3}. The radius of the spheres is $S = 0.358\ \mu$m and they occupy the sites of an fcc lattice with the same lattice constant as for the polaritonic crystal ($a = 1.264\ \mu$m).

In figure 3(a) we show the effective relative dielectric permittivity $\epsilon_{\rm eff}$ as calculated by equations (2) and (4). Despite $\epsilon(\omega)$ of the n-type Ge spheres (6) being negative for $\omega < \omega_{\rm p} = \omega_{\rm T}$, the real part of the effective relative dielectric permittivity $\epsilon_{\rm eff}$ of the composite assumes negative values only from $\omega/\omega_{\rm T} = 0.893$ to 0.977, resulting in a frequency gap. In figure 3(b) we show the frequency band structure of the infinite fcc crystal as calculated by the LKKR method, for $\mathbf{k}_\| = \mathbf{0}$. As for the case of the polaritonic crystal of figure 2, the crystal is viewed as a succession of planes parallel to the (001) surface. The frequency gap resulting from the frequency band structure obtained by the LKKR method extends from $\omega/\omega_{\rm T} = 0.909$ to 0.938, which is narrower than the frequency gap predicted by the effective medium theory (see figure 3(a)). It should not come as surprise that, despite relatively high filling fraction

f, ϵ_{eff} is not necessarily negative over all frequency range in which $\epsilon_{\mathrm{s}} < 0$. Indeed, as any textbook says, the effective relative dielectric permittivity ϵ_{eff} is determined by the single-sphere polarization factor. In the static case, the latter is given by $\alpha_{\mathrm{s}} = (\epsilon_{\mathrm{s}} - \epsilon_{\mathrm{h}})/(\epsilon_{\mathrm{s}} + 2\epsilon_{\mathrm{h}})$. Therefore, irrespective of whether ϵ_{s} is plus or minus infinity, one has $\alpha_{\mathrm{s}} = 1$. On the other hand, starting from the Maxwell–Garnett formula (1), one finds that ϵ_{eff} is negative if and only if either $\alpha_{\mathrm{s}} > (1/f)$ or $\alpha_{\mathrm{s}} < -1/(2f)$. Therefore, contrary to naive expectations, the negative effective permittivity ϵ_{eff} of the composite is to be expected not at extremely large negative values of ϵ_{s} but rather at moderately negative values of ϵ_{s}. This is exactly what has been confirmed by our analysis. Given equation (6), the relative dielectric permittivity of the spheres is in the range $0 > \epsilon_{\mathrm{s}} \gtrsim -3.7$ for $\omega/\omega_{\mathrm{T}} \in (0.9, 1)$ in figure 3.

Next to the band structure, in figure 3(c), we show the transmission coefficient of light incident normally on a slab of the crystal consisting of 16 planes of spheres parallel to the (001) surface. The transmittance is attenuated within the region of the frequency gap while it exhibits a rather spiky spectrum for frequencies above the gap up to $\omega/\omega_{\mathrm{T}} \approx 0.975$. The band gap of figure 3(b) overlaps with the frequency band of the polaritonic crystal of figure 2(b). Therefore, we suspect that if we create a crystal which will consist of spheres of both types, i.e., polaritonic and plasma spheres, it will exhibit a negative refractive index in the common region of both band gaps. Of course, the interaction between the resonance states of the spheres (of the same or different kinds) will modify the width as well as the centre of the gap; but we expect that a left-handed transmittance peak will emerge somewhere within the overlap region of the two band gaps.

4.2. Negative refractive index structures

In what follows, we shall consider a crystal consisting of alternating planes of polaritonic and plasma spheres (multilayer structure) and prove, both using the extended Maxwell–Garnett effective medium theory and the rigorous LKKR method, that the expectations raised at the end of the preceding section are valid. As usual, the slab of the multilayer crystal is viewed as a succession of two-dimensional photonic crystal planes of spheres along the [001] direction of an fcc lattice. However, now the spheres are the same only every second plane. The respective spheres are identical with those of figures 2 and 3. Thus the resulting structure can also be visualized as two interpenetrating *simple cubic* lattices of the respective polaritonic $LiTaO_3$ and Drude-like n-type Ge spheres characterized in that, when the differences between the spheres are ignored, the spheres are arranged on an fcc lattice.

The effective medium parameters of a composite comprising different spheres embedded in a matrix can be obtained from the condition that the average extinction of random unit cells compared with that of the surrounding medium is zero, i.e., the *average forward scattering amplitude* is zero, $\bar{S}(0) = 0$ [48]. For a composite comprising two different kinds of spheres embedded in a matrix (binary composite) one finds

$$p_{\mathrm{A}} \frac{\epsilon_{\mathrm{h}} - \epsilon_{\mathrm{eff}} - \frac{3\mathrm{i}}{2x^3} T^{\mathrm{E}}_{1,\mathrm{A}} f_{\mathrm{AB}} (2\epsilon_{\mathrm{h}} + \epsilon_{\mathrm{eff}})}{\epsilon_{\mathrm{h}} + 2\epsilon_{\mathrm{eff}} - \frac{3\mathrm{i}}{x^3} T^{\mathrm{E}}_{1,\mathrm{A}} f_{\mathrm{AB}} (\epsilon_{\mathrm{h}} - \epsilon_{\mathrm{eff}})} + p_{\mathrm{B}} \frac{\epsilon_{\mathrm{h}} - \epsilon_{\mathrm{eff}} - \frac{3\mathrm{i}}{2x^3} T^{\mathrm{E}}_{1,\mathrm{B}} f_{\mathrm{AB}} (2\epsilon_{\mathrm{h}} + \epsilon_{\mathrm{eff}})}{\epsilon_{\mathrm{h}} + 2\epsilon_{\mathrm{eff}} - \frac{3\mathrm{i}}{x^3} T^{\mathrm{E}}_{1,\mathrm{B}} f_{\mathrm{AB}} (\epsilon_{\mathrm{h}} - \epsilon_{\mathrm{eff}})} = 0, \tag{7}$$

where f_{AB} is the total filling factor of the spheres and the respective p_{A} and $p_{\mathrm{B}} = 1 - p_{\mathrm{A}}$ are the probabilities of occurrence of the spheres A and B. In deriving equation (7) it has been assumed that the respective random unit-cell volumes of spheres A and B are proportional to the A and B sphere radii. Equation (7) is an extension of equation (8) of [48] to the quasi-static limit, and it provides a generalization of the earlier expression for the effective relative dielectric permittivity, equation (2), to the two-sphere composite. An extension of equation (3) for the effective relative magnetic permeability of a binary composite can be obtained by replacing in

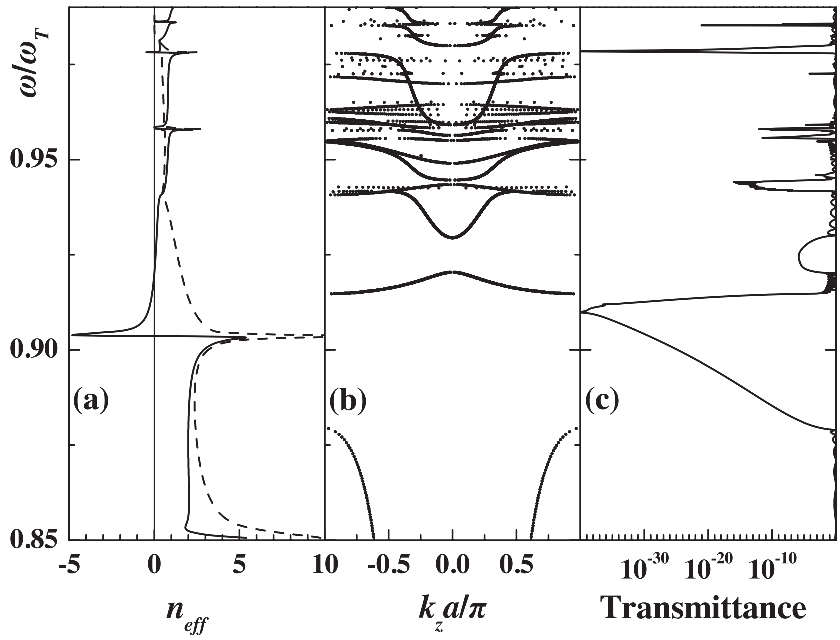

Figure 4. (a) The real (solid line) and imaginary (broken line) parts of n_{eff} within the extended Maxwell–Garnett theory and (b) the frequency band structure for $\mathbf{k}_{\|} = \mathbf{0}$ of a crystal consisting of alternating planes of $LiTaO_3$ and n-type Ge spheres which occupy the sites of an fcc lattice as calculated by the rigorous LKKR method. The planes of spheres are parallel to the (001) surface of an fcc crystal and the $LiTaO_3$ (n-type Ge) spheres have the same radius as those of figure 2 (figure 3). (c) The corresponding transmittance curve for light incident normally on a slab of the above crystal. The slab consists of 8 layers (one layer contains two planes of spheres, one from each kind). In the present case, the negative refractive index band central frequency of $\omega_{\mathrm{c}} = 0.9175\omega_{\mathrm{T}}$ corresponds to the wavelength of $\lambda_{\mathrm{c}} \simeq 12.238\ \mu$m. Therefore, the resulting structure is a truly subwavelength structure with the wavelength-to-structure ratio almost 14:1.

equation (7) the respective dielectric permittivities with corresponding magnetic permeabilities and the T_1^{E} matrix elements with corresponding T_1^{H}.

Equation (7) yields a quadratic equation for ϵ_{eff}, which can be easily solved, and analogously for μ_{eff}. The resulting refractive index $n_{\mathrm{eff}} = \sqrt{\epsilon_{\mathrm{eff}}\mu_{\mathrm{eff}}}$ for $p_{\mathrm{A}} = p_{\mathrm{B}} = 0.5$ is plotted in figure 4(a). The complex index of refraction is given by the branch of the square root that yields a non-negative imaginary part of n_{eff} along the positive real frequency axis. The region of negative refractive index is found to be centred at mid-wavelengths of 12331 nm with band width of 205 nm (1.6%). Note in passing that ϵ_{eff} and μ_{eff} are not necessarily both negative within the negative refractive index region.

The effective medium results are compared against the rigorous LKKR method calculations in figures 4(b), (c). Figure 4(b) shows the frequency band structure of the infinite multilayered crystal for $\mathbf{k}_{\|} = \mathbf{0}$. We see that there exist two main frequency gaps: the first from $\omega/\omega_{\mathrm{T}} = 0.88$ to 0.915 and the second from $\omega/\omega_{\mathrm{T}} = 0.92$ to 0.929. Between these two gaps there exists a frequency band extending from $\omega/\omega_{\mathrm{T}} = 0.915$ to 0.92 where the group velocity $v_{\mathrm{g}} = \partial\omega/\partial k_z$ has the opposite sign to the phase velocity $v_{\mathrm{p}} = \omega/k_z$. This effect is the signature of negative refraction and consequently of negative refractive index [49]. The left-handed band corresponds to a (left-handed) peak of the transmittance of light from a finite multilayer slab (see figure 4(c)). Note that this left-handed frequency band is *doubly degenerate* (optically

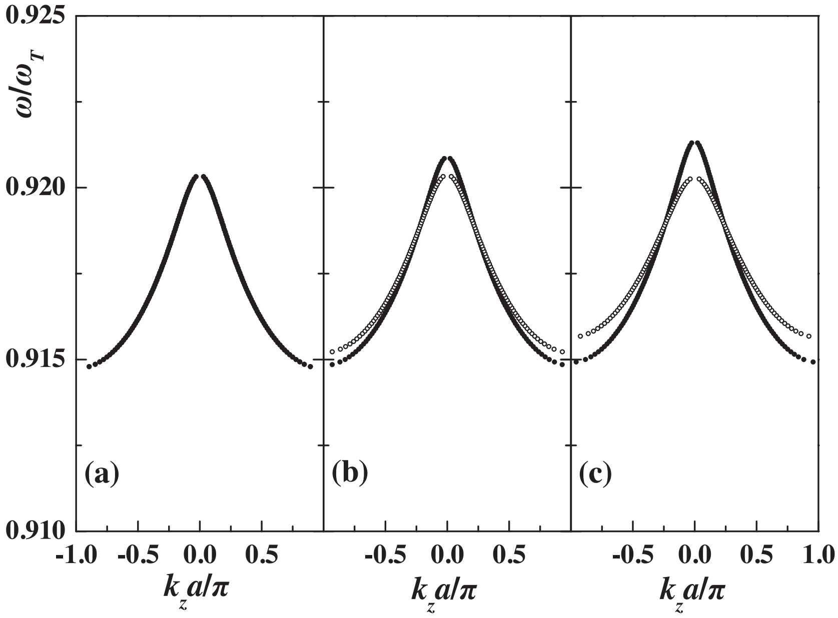

Figure 5. Negative index bands of the structure of figure 4 for (a) $\mathbf{k}_\parallel = \mathbf{0}$, (b) $\mathbf{k}_\parallel = (2\pi\omega_T/c)(0.1456, 0)$, and (c) $\mathbf{k}_\parallel = (2\pi\omega_T/c)(0.103, 0.103)$. The open (full) circles correspond to the bands which couple with an s-p-polarized incident plane wave.

active) and therefore couples with a normally incident EM plane wave. This is in contrast to the case of the polaritonic crystal (see figure 2) where, although the band from $\omega/\omega_T = 0.934$ to 0.949 exhibits negative refraction as well, it does not allow for efficient coupling with externally incident light due to its longitudinal nature (singly degenerate band). The refractive index, $n = -ck_z/\pi$, which corresponds to the left-handed band varies monotonically from $n = -4.859$ at the low-frequency edge of the band to $n = 0$ at the higher edge and assumes the value $n = -1$ at $\omega/\omega_T = 0.9187$. The latter value is required for the operation of a perfect planar lens [8].

The results presented so far correspond to normal incidence, i.e., for $\mathbf{k}_\parallel = \mathbf{0}$. The question that arises naturally is whether the left-handed band exists for other (non-zero) values of $\mathbf{k}_\parallel$ or not. Effective medium theory provides a refractive index which is isotropic and independent of $\mathbf{k}_\parallel$ (see figure 4(a)). In figure 5 we show the left-handed band as obtained from the rigorous LKKR method for three different values of $\mathbf{k}_\parallel$. Figure 5(a) corresponds to normal incidence $\mathbf{k}_\parallel = \mathbf{0}$. In figures 5(b) and (c), the $\mathbf{k}_\parallel$-values are chosen so that they correspond to the maximum allowed magnitude of $\mathbf{k}_\parallel$, $|\mathbf{k}_\parallel| = 0.1456(2\pi\omega_T/c)$ for $\omega/\omega_T = 0.915$ (lower edge of the negative index band for $\mathbf{k}_\parallel = \mathbf{0}$). For values of $|\mathbf{k}_\parallel|$ beyond $|\mathbf{k}_\parallel| = 0.1456(2\pi\omega_T/c)$ there is no propagating incident wave for this specific frequency. The vector $\mathbf{k}_\parallel = (2\pi\omega_T/c)(0.1456, 0)$ is parallel to the $\overline{\Gamma X}$ line and $\mathbf{k}_\parallel = (2\pi\omega_T/c)(0.103, 0.103)$ is parallel to the $\overline{\Gamma M}$ line of the (001) surface Brillouin zone (SBZ). We observe that for $\mathbf{k}_\parallel \neq \mathbf{0}$ the left-handed band experiences a weak birefringent splitting into two different bands according to the polarization of an incident plane wave: the band depicted with the open circles couples with s-polarized incident waves, whilst the one depicted with full circles couples with p-polarized incident waves. The position, width and shape of both left-handed bands vary only slightly with $\mathbf{k}_\parallel$, rendering negative refraction in the proposed metamaterial feasible.

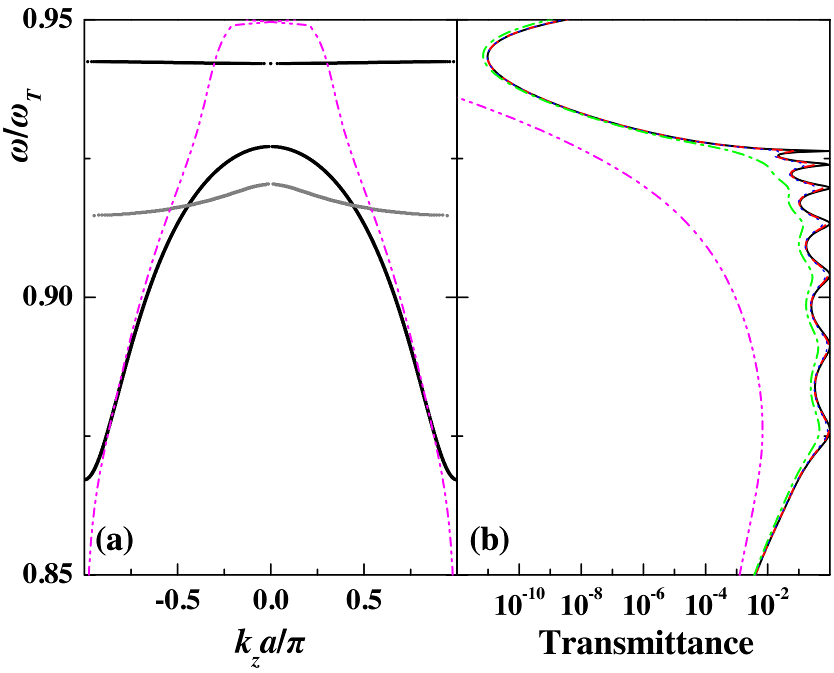

Figure 6. (a) The same as figure 4(b) but for $\epsilon_{\rm h} = 12$ with a rescaled radius of Ge spheres by the factor of $1/\sqrt{\epsilon_{\rm h}}$ and the frequency region from $\omega/\omega_{\rm T} = 0.85$ to 0.95. For a comparison, the negative refractive index band for $\epsilon_{\rm h} = 1$ of figure 4(b) is shown here with a thin line. The dash–double dotted line corresponds to the frequency band with the smallest imaginary part of k_z when we restore the actual values of the loss factors in constituent materials, i.e., $\gamma_1 = 5.9$ THz and $\gamma_2 = 10$ THz in equations (5) and (6). (b) The corresponding transmittance curves for light incident normally on a slab of 8 layers, for various values of the loss factors γ_1 and γ_2: $\gamma_1 = 0$ and $\gamma_2 = 0$ (solid), $\gamma_1 = 0.059$ THz ($\gamma_1 \approx \omega_{\rm T}/3000$) and $\gamma_2 = 0.1$ THz ($\gamma_2 \approx \omega_{\rm p}/1500$) (dashed), $\gamma_1 = 0.118$ THz ($\gamma_1 \approx \omega_{\rm T}/1500$) and $\gamma_2 = 0.2$ THz ($\gamma_2 \approx \omega_{\rm p}/750$) (dotted), $\gamma_1 = 0.59$ THz ($\gamma_1 \approx \omega_{\rm T}/300$) and $\gamma_2 = 1$ THz ($\gamma_2 \approx \omega_{\rm p}/150$) (dash–dotted), $\gamma_1 = 5.9$ THz ($\gamma_1 \approx \omega_{\rm T}/30$) and $\gamma_2 = 10$ THz ($\gamma_2 \approx \omega_{\rm p}/15$) (dash–double dotted).

(This figure is in colour only in the electronic version)

The structure discussed above has one shortcoming: since $\epsilon_{\rm h} = 1$ it requires the spheres to be suspended in air. In order to provide a manufacturable structure we have investigated the influence of the dielectric constant $\epsilon_{\rm h}$ of the surrounding medium on the properties of the negative refractive index band. As shown in figure 6(a), assuming a non-magnetic embedding medium (ambient) with refractive index $n_{\rm h} = \sqrt{\epsilon_{\rm h}}$, the main conclusions about the existence and position of the negative refractive index band remain invariant provided that the Ge sphere radius is scaled down by a factor of $1/n_{\rm h}$. An unexpected and surprising bonus effect is a dramatic increase of the negative refractive index bandwidth with increasing $n_{\rm h}$. For instance, the bandwidth increases from 0.5% for $n_{\rm h} = 1$ up to 6.7% for $n_{\rm h} = \sqrt{12} \approx 3.46$, i.e., by a factor of more than 13. Note in passing that the negative refractive index bandwidth can also be tuned by detuning $\omega_{\rm p}$ a few per cent away from $\omega_{\rm T}$.

We stress that the metamaterials under study are *subwavelength* structures since the wavelength of light $\lambda_{\rm c} \approx 12.238$ μm in the negative refractive index region is almost *ten times* larger than the fcc lattice constant a ($\lambda_{\rm c}/a = 12.238/1.264 \approx 9.6$). Since the shortest distance between spheres in an fcc lattice is identical to the lattice constant $a_0 = a/\sqrt{2}$ of the square lattice corresponding to a (001) plane, the resulting wavelength-to-structure ratio λ_c/a_0 is approximately 14:1.

5. Effect of absorption

So far we have neglected the losses in both the polaritonic and Drude-like materials which constitute the proposed metamaterial composite. Correspondingly, the loss factors in equations (5) and (6) have been kept zero till now. (It is recalled here that the non-zero imaginary part of the effective medium constants in the quasi-static approximation displayed in figures 2(a), 3(a) and 4(a) is a direct measure of the normally propagating beam attenuation due to the scattering and is not associated with any absorption or the heating rate [21, 29].) In the present section, the influence of absorption of the constituent materials on the properties of the resulting structure is studied. For $LiTaO_3$ the loss factor is $\gamma_1 = 5.9$ THz [30], i.e., one should set $\gamma_1 \approx \omega_T/30$ in equation (5). A typical value of γ_2 for a semiconductor is $\gamma_2 = 10$ THz [50], i.e., in our case of n-doped Ge, $\gamma_2 \approx \omega_p/15$ in equation (6). However, there are only very few polaritonic materials whose dielectric constant has been accurately determined in the far infrared and at terahertz frequencies [30, 35]. Therefore, in the absence of available experimental data, we shall, similarly as in [35], consider a range of values of the loss factors. Hopefully, those loss values will turn interesting with respect to other polaritonic materials, such as SiC, TlBr, TlCl, which have ω_T ranging from 8.1 to 149 THz [30, 35]. For instance, Huang *et al* [35] speculated that SiC, whose ω_T is approximately six times larger than that of $LiTaO_3$, can have γ_1 as low as $\approx\omega_T/300$. Note in passing that the matching of the frequencies ω_T and ω_p involves tuning of the doping level of n-type Ge which, in effect, alters the amount of the loss factor γ_2 [45].

The full circles (solid line) of figure 6(a) correspond to the frequency band structure, in the absence of absorption, similarly to figure 4(b), but for $\epsilon_h = 12$, the radius of Ge spheres scaled down by a factor of $1/\sqrt{\epsilon_h}(=1/n_h)$, and the frequency region from $\omega/\omega_T = 0.85$ to 0.95. For a comparison, the negative refractive index band for $\epsilon_h = 1$ of figure 4(b) is shown here with a thin line. When the loss factors assume their actual values, i.e., $\gamma_1 = 5.9$ THz and $\gamma_2 = 10$ THz, we obtain the dash–double dotted line of figure 6(a). We know that there are no frequency bands corresponding to propagating solutions of the infinite crystal in the presence of losses. Nevertheless, we can still define a frequency band which determines the coupling of an external wave with a finite slab of the crystal; namely, the frequency band which corresponds to the smallest imaginary part of k_z. This is the band which is depicted with the dash–double dotted line in figure 6(a). By inspection of this band we confirm that, even in the presence of absorption, the negative index is the dominant one (i.e., the one with the smallest imaginary part of k_z) and will therefore determine the transmission and absorption of externally incident light. This ensures the occurrence of negative refraction in the presence of losses as a consequence of a refractive index with negative real part.

Next to the band structure curves of figure 6 we show the transmission for normally incident light on our multilayer slab consisting of 16 planes of spheres embedded in a host with $\epsilon_h = 12$ for various values of the loss factors. For low values of γ_1 and γ_2 (dashed and dotted curves) the transmittance remains almost unaffected by the presence of absorption. However, for higher values of the loss factors (dash–dotted curve) the abrupt features of the transmission curve smooth out and transmission within the left-handed band is reduced by almost two orders of magnitude on the average. When the actual loss factors are assumed (dash–double dotted curve) the transmittance is considerably suppressed and the spectral gap around $\omega/\omega_T = 0.942$ is widened, reducing even more the transmittance in the left-handed band. Perhaps for other choices of materials (with smaller loss factors) transmittance would be relatively larger in the left-handed band. However, the experimentalist can still observe negative refraction in the theoretically predicted frequency region of the left-handed band even if the measured transmission can be rather low. As has been reported many times before, losses are the most demanding problem to cope with in designing a functional metamaterial.

6. Discussion

6.1. The origin of negative refractive index band

We should mention that the frequency region within which our metamaterials exhibit left-handed behaviour is much *narrower* than the region where $\epsilon_{\rm eff}$ of the sublattice of Drude-like spheres and $\mu_{\rm eff}$ of the polaritonic sublattice simultaneously become negative. Indeed, according to figures 2 and 3, the region from $\omega/\omega_{\rm T} = 0.900$ to 0.948, where both $\mu_{\rm eff}$ and $\epsilon_{\rm eff}$ are negative, is much *broader* than left-handed band index band ($\omega/\omega_{\rm T} = 0.915$ to 0.92 in figure 4). This is due to the fact that, since we have chosen the plasma frequency of the n-type Ge spheres to coincide with the optical phonon frequency of $LiTaO_3$, a considerably strong interaction between the resonance states of spheres of the two different constituent materials occurs. The latter drastically affects the formation of a left-handed band. For example, had we taken plasma spheres of the same radius as the polaritonic ones, there would be no left-handed band in the frequency band structure of multilayer crystal in contrast to what is expected from simply taking the overlap of the negative $\epsilon_{\rm eff}$- and $\mu_{\rm eff}$-frequency regions. Similar phenomena have been observed in metamaterials consisting of SRRs combined with thin metallic wires [51, 52].

A folklore says that both $\epsilon_{\rm eff}$ and $\mu_{\rm eff}$ of a given structure have to be negative in order for the structure to possess a negative refractive index. That has also been our guiding principle in designing our negative refractive index structures. This principle is also true provided the respective imaginary parts of $\epsilon_{\rm eff}$ and $\mu_{\rm eff}$ are very small compared to the real parts. Indeed, assuming the complex plane cut along the real positive axis, the product $\epsilon_{\rm eff}\mu_{\rm eff}$ is then a complex number lying in the fourth quadrant closely below the real positive axis. The only physical restriction on selecting the branch of the square root $\sqrt{\epsilon_{\rm eff}\mu_{\rm eff}}$, which yields the complex index of refraction, is that $n_{\rm eff}$ has to have a *non-negative imaginary part* (along the positive real frequency axis). This condition then selects $\sqrt{\epsilon_{\rm eff}\mu_{\rm eff}}$ in the second quadrant slightly above the negative real axis. However, a different situation occurs if the imaginary part of at least one of $\epsilon_{\rm eff}$ and $\mu_{\rm eff}$ becomes comparable to the real part. Then it may be sufficient that the real part of merely one of $\epsilon_{\rm eff}$ and $\mu_{\rm eff}$ is negative in order that the real part of $n_{\rm eff}$ be negative. For instance, let $\mathrm{Re}\,\mu_{\rm eff} \simeq \mathrm{Im}\,\mu_{\rm eff} > 0$. Then, for $\mathrm{Re}\,\epsilon_{\rm eff} \lesssim -\mathrm{Im}\,\epsilon_{\rm eff}$ (a condition which can readily be achieved using Drude-like materials), the product $\epsilon_{\rm eff}\mu_{\rm eff}$ is a complex number lying in the third quadrant of the complex plane (such is, for instance, the product of *non-magnetic* $\mu_{\rm eff} = 1 + \mathrm{i}$ and $\epsilon_{\rm eff} = -2 + 0.1\mathrm{i}$). The physical square root of the product $\epsilon_{\rm eff}\mu_{\rm eff}$ is then within the second quadrant of the complex plane implying a negative real part of $n_{\rm eff}$, the complex index of refraction. Therefore, the negative refractive index region does not necessarily imply that both $\epsilon_{\rm eff}$ and $\mu_{\rm eff}$ are negative. An interesting recent article by Luo *et al* [53] suggests even the possibility of an all-angle negative refraction effect without the negative refractive index.

6.2. Related work

Earlier work on subwavelength negative refractive index metamaterials have mostly focused on complicated structures comprising split ring resonators and wires [14–18]. Although these structures do work for microwaves, it is difficult to imagine that they can be scaled down several orders of magnitude in size and provide a negative refractive index metamaterial for terahertz or even infrared regions. Instead, our proposal for a negative refractive index structure, which expands on that by Holloway *et al* [28], only involves arrays of spherical particles embedded in a matrix. This opens up the possibility of fabricating *homogeneous* and *isotropic* negative refractive index metamaterials much more simply than has been proposed up until now.

Our work differs from the negative refractive index metamaterial of Holloway *et al* [28], which comprised a mixture of *magnetodielectric* spheres, in that inherently magnetic materials are *not* required. This is a key difference which makes it possible to achieve a negative refractive index band down to the deep infrared region. Note that materials that exhibit magnetic response are (i) particularly rare at terahertz and infrared frequencies and, if they exist, (ii) they usually suffer from high losses. Magnetic polarization in materials follows indirectly either from the flow of orbital currents or from unpaired electron spins. In magnetic systems, resonant phenomena, analogous to the phonons or collective modes that lead to an enhanced electric response at infrared or higher frequencies, tend to occur at far lower frequencies, resulting in relatively little magnetic material response at terahertz and higher frequencies.

The idea of generating an effective magnetic response from a composite comprising inherently non-magnetic materials is not new, and has been already implicit in the work of Lewin [27] and explicit in Khizhnyak [54] (see also [28] for an extended historical survey). More recently, the idea has been rejuvenated in [1, 2, 31, 35]. However, the proposal of creating a negative refractive index medium as a multilayer of alternating layers of non-overlapping spheres from inherently non-magnetic polaritonic and Drude-like materials appears to be novel. The proposed negative refractive index material is a truly subwavelength structure with wavelength-to-structure ratio as high as 14:1. This is not case in the negative refraction observed in purely dielectric metamaterials, where wavelengths in the left-handed band are comparable to the period of the structure [9, 10]. The wavelength-to-structure ratio of our structures is almost 50% higher than has been previously achieved using the most popular metamaterials consisting of split ring resonators (SRRs) and wires [14–18].

6.3. Periodic versus aperiodic realizations

Although the required sphere filling fraction is rather high (at least $\approx$38%), it has been found that already the static Maxwell–Garnett theory (1) may yield effective medium properties, for frequencies till the first stop gap, within a few per cent of the exact result even for nearly close-packed cubic photonic crystals [36]. Given that our structure is a truly subwavelength structure with wavelength-to-structure ratio as high as 14:1 and that the quasi-static results (see figures 2(a), 3(a) and 4(a)) provide a very reasonable approximation to the rigorous results obtained using a well documented computer code based on the LKKR method [22–24] (see figures 2(b) and (c), 3(b) and (c), 4(b) and (c)), this strongly suggest that the periodicity of section 4 is not necessary and a negative refractive index metamaterial can also be obtained as an *aperiodic* or *disordered* structure.

As alluded to earlier, the imaginary part of the effective medium constants in the quasi-static approximation is no longer a direct measure of the absorption or the heating rate [21, 29]; yet it is still a measure of the beam attenuation due to a combined effect of the scattering and absorption. Not surprisingly, the resulting beam attenuation within the negative refractive index band is expected to be stronger in the aperiodic case than in the periodic case. However, the aperiodic case can be fabricated much more easily and, if relatively thin layers of the negative refractive index metamaterial are required, the aperiodic realization of our structure can still be a viable alternative.

6.4. Fabrication

Given that available polaritonic materials, such as SiC, $LiTaO_3$, TlCl, TlBr, have ω_T between 8.1 to 149 THz [30, 35], the required particle (sphere) radii are typically between 80 nm (SiC) and 1.47 μm (TlBr). Therefore, all these negative refractive index metamaterial possibilities are amenable to fabrication using either colloidal techniques [39, 40] or micromanipulation (for instance, using optical tweezers or microrobots) [36]. In the former case, the (111) stacking of an fcc lattice, which corresponds to the stacking of two-dimensional *hexagonal* lattice layers of spheres, is of particular importance. Although our results have only been presented for the (001) stacking of two-dimensional *square* lattice layers of spheres, the main conclusions also remain valid for the (111) stacking, or any other stacking of an fcc structure. This is because the resulting wavelength-to-structure ratio λ_c/a_0 is as high as 14:1. Hence the particular choice of the crystal structure or its stacking is not important as long as the crystal has cubic symmetry, which ensures that the effective medium properties are *homogeneous* and substantially *isotropic* (see figure 5).

The fabrication of our negative refractive index metamaterial (using either colloidal techniques or micromanipulation) can be facilitated, for example, by first coating the respective $LiTaO_3$ and n-type Ge spheres with the same (non-magnetic) material so that the respective radii of coated spheres become identical. (For experiments involving photonic crystals of silica-coated semiconductor (ZnS) spheres see [39].) This would make the subsequent sphere assembly, either in the periodic or aperiodic case, much easier. A final step would be then to fill in the resulting interstices with a material with a refractive index matching that of the sphere-coating material. Note that an isolating coating layer on the respective $LiTaO_3$ and n-type Ge spheres would also provide for an electric isolation of the respective spheres. The latter feature is of utmost importance for the validity of the effective medium theory presented in section 4.2.

6.5. Outlook

In designing our negative refractive index metamaterial as a stack of alternating two-dimensional photonic crystals layers of non-overlapping spheres from inherently *non-magnetic* polaritonic and Drude-like materials, respectively, we have followed the route of making elementary components (spheres) simple at the expense of making the photonic crystal structure complex (not a simple Bravais lattice). An alternative approach might be to keep the photonic crystal structure simple (e.g., simple fcc). The price to pay would be to employ complex elementary components, i.e., multicoated spheres. Furthermore, the proposed negative refractive index metamaterials may also consist of spheroidal or cylindrical particles.

We have shown in figure 6(a) that the negative refractive index bandwidth increases from 0.5% for $n_h = 1$ up to 6.7% for $n_h = \sqrt{12} \approx 3.46$, i.e., by more than a factor of 13. Note in passing that the negative refractive index bandwidth can also be tuned by detuning ω_p by a few per cent away from ω_T. Occasionally, by a proper detuning, the negative refractive index band can almost double its width. These routes will be followed elsewhere.

The transmission properties of our negative refractive index structures have not yet been optimized. In this regard, reference [53] suggests that by requiring a negative refractive index slab to possess both mirror symmetry and a thickness equal to an integer multiple of half the wavelength in the slab, reflections can be minimized and transmission above 99% can be achieved.

7. Conclusions

Mere magnetic response of materials at terahertz and infrared frequencies is important for the implementation of devices such as compact cavities, adaptive selective lenses, tunable mirrors, isolators, converters, optical polarizers, filters, and phase shifters [1, 2]. Motivated by this, we have proposed a new set of artificial structures which not only exhibit magnetic response (see section 3) but can also possess a negative refractive index band in excess of 6% within a broad range, i.e., from the deep infrared to the terahertz (1–10 THz) region.

The favoured realization of our structure is a periodic crystal wherein the respective polaritonic spheres and Drude-like, or plasma, spheres are arranged on two interpenetrating simple cubic lattices so that, when the differences between the spheres are ignored, the resulting structure is an fcc structure. Along the [001] fcc stacking direction the structures can be visualized as a stack of alternating two-dimensional photonic crystals layers of non-overlapping spheres from polaritonic and Drude-like materials, respectively. The optical properties of such negative refractive index multilayers comprising polaritonic and Drude-like spherical particles have been studied using both analytical and rigorous numerical techniques based on the photonic LKKR method. A very nice agreement between the extended Maxwell–Garnett theory and the LKKR method results has been established. The negative refractive index (left-handed) frequency band has been found doubly degenerate and as such it allows for efficient coupling with normally incident light. An illustrative example comprising $LiTaO_3$ and n-type Ge spheres revealed a negative refractive index centred around $\lambda_c \simeq 12.238\ \mu$m. By using other available polaritonic materials, such as SiC, TlBr, TlCl, which have ω_T ranging from 8.1 to 149 THz [30, 35], the centre wavelength λ_c of the negative refractive index band can be correspondingly tuned over a wide frequency range, provided the polaritonic component is combined with a properly doped n-type semiconductor (e.g., Ge) spheres, so that $\omega_p \simeq \omega_T$. The above choices of materials can lead to efficient optical components for terahertz beams, which are required in many scientific and technological applications, ranging from the imaging of biological materials to manipulating quantum states in semiconductors, from drug discovery and medical imaging to security screening [55]. The proposed negative refractive index material is a truly subwavelength structure with wavelength-to-structure ratio as high as 14:1, which is almost 50% higher than has been previously achieved [14–18]. Therefore, our structures exhibit improved homogeneous and isotropic properties in the negative refractive index band and are expected to be more robust against disorder.

In the search for suitable negative refractive index metamaterial one must not forget that, already, the possibility of having a metamaterial with an effective non-negative refractive index less than unity can have profound technological application as either a reflection or antireflection coating layer of various optical components, or as ultra-refractive optical components [56]. The latter can also be achieved by the proposed structures (see, e.g., figure 4(a)).

References

[1] Panina L V, Grigorenko A N and Makhnovskiy D P 2002 *Phys. Rev.* B **66** 155411
[2] Yen T J *et al* 2004 *Science* **303** 1494
[3] Veselago V G 1968 *Sov. Phys.—Usp.* **10** 509
[4] Silin R A 1972 *Izv. Vyssh. Uchebn. Zaved. Radiofiz.* **15** 809
Silin R A 1978 *Opt. Spektrosk.* **44** 189
[5] Pendry J B 2004 *Contemp. Phys.* **45** 191
[6] An extended historical overview going back before the work of Veselago can be found on http://www.wave-scattering.com/negative.html
[7] Zengerle R 1987 *J. Mod. Opt.* **34** 1589
[8] Pendry J B 2000 *Phys. Rev. Lett.* **85** 3966
[9] Foteinopoulou S, Economou E N and Soukoulis C M 2003 *Phys. Rev. Lett.* **90** 107402
[10] Cubukcu E, Aydin K, Ozbay E, Foteinopoulou S and Soukoulis C M 2003 *Nature* **423** 604
[11] Rotman W 1962 *IEEE Trans. Antennas Propag.* **10** 82

[12] Pendry J B, Holden A J, Stewart W J and Youngs I 1996 *Phys. Rev. Lett.* **76** 4773
[13] Pendry J B, Holden A J, Robbins D J and Stewart W J 1999 *IEEE Trans. Microw. Theory* **47** 2075
[14] Smith D R, Padilla W J, Vier D C, Nemat-Nasser S C and Schultz S 2000 *Phys. Rev. Lett.* **84** 4184
[15] Shelby R A, Smith D R and Schultz S 2001 *Science* **292** 77
[16] Parazzoli C G, Greegor R B, Li K, Koltenbah B E C and Tanielian M 2003 *Phys. Rev. Lett.* **90** 107401
[17] Houck A A, Bock J B and Chuang I L 2003 *Phys. Rev. Lett.* **90** 137401
[18] Markoš P and Soukoulis C M 2002 *Phys. Rev.* B **65** 033401
[19] Ziolkowski R W 2003 *Opt. Express* **11** 662
[20] Doyle W T 1989 *Phys. Rev.* B **39** 9852
[21] Ruppin R 2000 *Opt. Commun.* **182** 273
[22] Stefanou N, Karathanos V and Modinos A 1992 *J. Phys.: Condens. Matter* **4** 7389
[23] Stefanou N, Yannopapas V and Modinos A 1998 *Comput. Phys. Commun.* **113** 49
[24] Stefanou N, Yannopapas V and Modinos A 2000 *Comput. Phys. Commun.* **132** 189
[25] Waterman P C and Pedersen N E 1986 *J. Appl. Phys.* **59** 2609
[26] Abramowitch M and Stegun I A 1973 *Handbook of Mathematical Functions* (New York: Dover)
[27] Lewin L 1947 *Proc. Inst. Electr. Eng.* **94** 65
[28] Holloway C L, Kuester E F, Baker-Jarvis J and Kabos P 2003 *IEEE Trans. Antennas Propag.* **51** 2596
[29] Bohren C F 1986 *J. Atmos. Sci.* **43** 468
[30] Kittel C 1976 *Introduction to Solid State Physics* (New York: Wiley)
[31] O'Brien S and Pendry J B 2002 *J. Phys.: Condens. Matter* **14** 4035
[32] Smith D R, Vier D C, Kroll N and Schultz S 2000 *Appl. Phys. Lett.* **77** 2246
[33] Huang Y and Gao L 2003 *Phys. Lett.* A **318** 592
[34] Huang K C, Bienstman P, Joannopoulos J D, Nelson K A and Fan S 2003 *Phys. Rev. Lett.* **90** 196402
Huang K C, Bienstman P, Joannopoulos J D, Nelson K A and Fan S 2003 *Phys. Rev.* B **68** 075209
Gatzounis G and Stefanou N 2005 *Phys. Rev.* B at press
[35] Huang K C, Povinelli M L and Joannopoulos J D 2004 *Appl. Phys. Lett.* **85** 543
[36] Moroz A 2002 *Phys. Rev.* B **66** 115109
[37] Zhang W Y, Lei X Y, Wang Z L, Zheng D G, Tam W Y, Chan C T and Sheng P 2000 *Phys. Rev. Lett.* **84** 2853
[38] Vlasov Y A, Xiang-Zheng B, Sturm J C and Norris D J 2001 *Nature* **414** 289
[39] Velikov K P, Moroz A and van Blaaderen A 2002 *Appl. Phys. Lett.* **80** 49
[40] Velikov K P, Vos W L, Moroz A and van Blaaderen A 2004 *Phys. Rev.* B **69** 075108
[41] Ohtaka K and Tanabe Y 1996 *J. Phys. Soc. Japan* **65** 2265
Ohtaka K and Tanabe Y 1996 *J. Phys. Soc. Japan* **65** 2276
[42] Karathanos V 1998 *J. Mod. Opt.* **45** 1751
[43] Halevi P and Ramos-Mendieta F 2000 *Phys. Rev. Lett.* **85** 1875
[44] Sánchez A S and Halevi P 2003 *J. Appl. Phys.* **94** 797
[45] Schroeder D K 1990 *Semiconductor Material and Device Characterization* (New York: Wiley)
[46] Yannopapas V, Modinos A and Stefanou N 1999 *Phys. Rev.* B **60** 5359
[47] Moroz A 1999 *Phys. Rev. Lett.* **83** 5274
[48] Luo R 1997 *Appl. Opt.* **36** 8153
[49] Pendry J B 2004 *Science* **306** 1353
[50] Fox M 2001 *Optical Properties of Solids* (New York: Oxford)
[51] Koschny T, Kafesaki M, Economou E N and Soukoulis C M 2004 *Phys. Rev. Lett.* **93** 107402
[52] Koschny T, Markoš P, Smith D R and Soukoulis C M 2004 *Phys. Rev.* E **68** 065602(R)
[53] Luo C, Johnson S G, Joannopoulos J D and Pendry J B 2002 *Phys. Rev.* B **65** 201104(R)
[54] Khizhnyak N A 1957 *Sov. Phys.—Tech. Phys.* **27** 2014
Khizhnyak N A 1959 *Sov. Phys.—Tech. Phys.* **29** 604
[55] See, for instance, special issue on 1994 Terahertz electromagnetic pulse generation, physics, and applications *J. Opt. Soc. Am.* B **11** 2454
[56] Gralak B, Enoch S and Tayeb G 2000 *J. Opt. Soc. Am.* A **17** 1012